ANNALS OF PHYSICS: 7, 1–38 (1959)

Radiation from Hot Air

Part II. Shock Tube Study of Absolute Intensities

JAMES C. KECK, JOHN C. CAMM, BENNETT KIVEL, AND TUNIS WENTINK, JR.

Avco Research Laboratory, Everett, Massachusetts

The radiation emitted by shock-heated oxygen, nitrogen, and air has been studied in the wavelength range 2000 to 10,000A at temperatures from 4000 to 9000°K and densities from 0.01 to 10 times standard atmospheric. Both spectroscopic and photometric techniques were employed. The radiation consists of bands from O_2, N_2, N_2^+, and NO molecules, lines from O and N atoms and continuum Kramers radiation from O^-. Comparison of the experimental results with the theoretical expressions giving the wavelength, temperature and density dependence of the radiation gave electronic *f*-numbers for all the bands observed.

INTRODUCTION

The optical radiation from air is important in problems of hypersonic aerodynamics, atomic explosions and atmospheric physics. In addition, the electronic transition moments of molecules are fundamental quantities in spectroscopy and quantum physics. The present paper describes an experimental study of the radiation from air heated by shock waves which has applications to all these problems.

The general theory of the emission of radiation by atoms and molecules has long been the subject of intensive study and is described in many texts (*1–3*). While in principle the radiation is completely predictable from known quantum mechanical laws, in practice the theory must usually be normalized by comparison with experiment to obtain absolute intensities. This normalization was a central aim of the present work. In the case of molecules, which are the most intense source of radiation from air, it involves determination of the electronic transition probabilities or *f*-numbers. In interpreting our results we have relied heavily on theoretical work by Kivel *et al.* (*4*) (KMB) given in Part I of this paper and by Meyerott (*5*).

Emission spectra of molecules have previously been studied in arcs, flames, and electric discharges. These sources, in addition to being highly nonuniform, are far from thermodynamic equilibrium and cannot be used for quantitative studies of absolute intensities. Ovens, such as the King furnace, have been used with more success since they achieve thermal equilibrium except near openings in the oven walls. However, they are limited to temperatures below which the walls disintegrate; typically this is the sublimation temperature of carbon, ~4000°K.

Most of the quantitative measurements of *f*-numbers which have been reported to date have been made in absorption experiments carried out at room temperature (*6–8*). The fact that so few *f*-numbers for molecular bands are currently known attests to the difficulty of these experiments. Moreover, the extrapolation of room temperature results to high temperatures is uncertain because the vibrational transitions involved frequently differ and there is no a priori reason to expect the effective electronic *f*-number to be the same for all vibrational transitions (*9*).

The development of the shock tube (*10*, *11*) has made possible the quantitative study of both the emission and absorption of radiation in gases at high temperatures. Under appropriate conditions it is possible to produce a uniform sample of gas in thermodynamic equilibrium at accurately known temperature and pressure. The obvious disadvantage of the shock tube is that the conditions are transient, lasting only from 10 to 100 μsec. However, modern techniques in electronics and spectroscopy make it possible to obtain much valuable data even in this short time interval, and the advantages of the shock tube in other respects are sure to promote the further development of new and more powerful techniques.

The versatility of the shock tube in spectroscopy is demonstrated by previously published work. Kantrowitz and co-workers (*12*) at Cornell University have measured the absolute emission intensity due to argon recombination or Kramers radiation ($A^+ + e \rightarrow A^* + h\nu$). At the same time they observed a shift of the argon spectral lines attributed to perturbations by the free electrons in the high temperature argon gas. Laporte and co-workers (*13*, *14*) at the University of Michigan have been making careful measurements of the spectral line profiles of hydrogen Balmer lines to determine the contribution of free electrons to the line broadening. Seay and Seely (*15*) at Los Alamos have studied helium using an explosive driver to obtain the required temperatures and Model (*16*) in Russia has used the same technique to study air. At the Cornell Aeronautical Laboratory (*17*, *18*) measurements of absorption by O_2 and air behind shock waves are being made. Exploratory studies have also been reported by Gaydon (*19*) and Nicholls (*20*). This list is not meant to be complete as there is much other work in progress.

The present studies owe their existence to the importance of radiative heat transfer in hypersonic aerodynamics. Practical considerations, therefore, played an important role in determining the conditions under which the gases were studied. The temperature range from 4000 to 9000°K and the initial density range from 0.001 to 1 times standard atmospheric density are appropriate in problems of hypersonic flight at speeds up to the satellite velocity. Most of the data on air were accumulated in the spring of 1956, but some data accumulated as a by-product of other studies carried out since then have also been included. In general, it was found that the internal consistency of the data obtained during a given experiment was ±20% while the maximum spread between experiments was ±30%. Considering the newness of the shock tube as a radiation research tool, the ability to reproduce results to this accuracy over so long a period of time is most gratifying, especially when one considers that this was a period of rapid growth in the understanding of shock tube performance. It should be emphasized, however, that even at the present writing our understanding of many important details of shock tube operation, particularly those associated with decelerating shock waves, is far from complete; therefore, there is a possible source of systematic error in the results.

The paper is divided into five parts: The first is devoted to a description of the shock tube and the general characteristics of the shock waves studied. The second describes the spectrographic work which resulted in the identification of the important radiating bands. The third describes the photometric studies from which absolute intensities were deduced. The fourth outlines the theory of the average emissivity of molecules and describes the reduction of data to *f*-numbers. The fifth is devoted to a discussion of the results and comparison with other work.

I. THE SHOCK TUBE

A schematic diagram of the shock tube used for the present measurements is shown in Fig. 1. The shock tube consisted of a high-pressure driver section separated from a low-pressure test section by a copper or steel diaphragm. The driver section was stainless steel tubing three feet long and 1½ inches inside diameter. The test section was 10 feet long and 1½ inches inside diameter. For the study of incident shock waves the test section was Pyrex tubing. It was not practical to use a Pyrex tube with reflected shock waves except in cases where extreme purity was required, since reflected shock waves exploded the tube on each run. A stainless steel test section was therefore employed for normal running. A photograph of the shock tube with the Pyrex tube in place is shown in Fig. 2.

Shock speeds up to 3.5 mm/μsec were obtained by using hydrogen in the driver

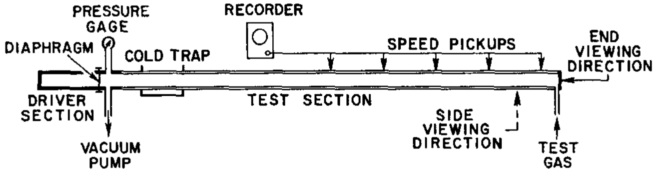

FIG. 1. Schematic diagram of shock tube.

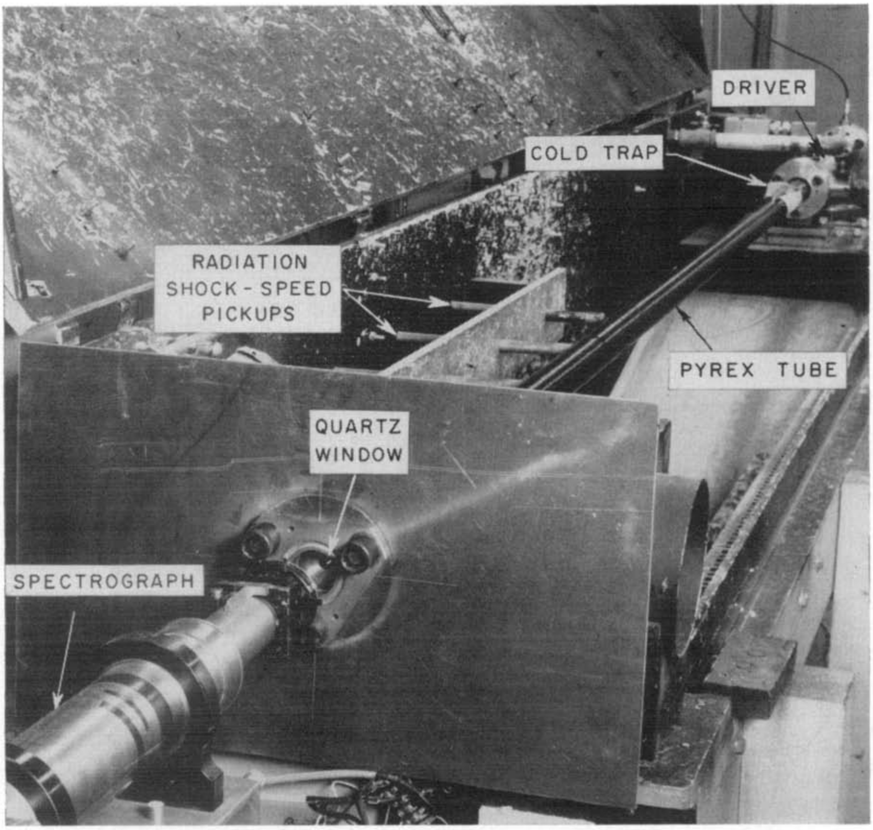

FIG. 2. Photograph of shock tube with Pyrex test section installed. Note the scars on the inside of the wooden box used to contain the fragments of the tube, which usually exploded after reflected shock runs.

at pressures up to 2000 psi. Faster shock speeds up to 6 mm/μsec were obtained by charging the driver with a stoichiometric mixture of H_2 and O_2 diluted with He and igniting the charge uniformly with an electrically-exploded aluminum wire running axially the length of the driver.

The test section was evacuated prior to introducing the test gas by a carefully trapped oil diffusion pump. With a Pyrex tube, pressures of less than 0.1 micron and virtual leak rates of less than 1 micron per minute were obtained by pumping for a few hours. With a stainless steel tube, pressure of a few microns with virtual leak rates of the order of 20 microns per minute were obtained.

To minimize impurities due to outgassing of walls a flow system was usually employed which changed the gas in the test section approximately 5 times a second. Before entering the shock tube the test gas was dried by passage through a dry ice or liquid N_2 trap. Check valves were employed to protect the flow system. In cases where the highest gas purity was sought the Pyrex tube with a liquid N_2 cold trap was employed as an alternative to the flow system. The cold trap was approximately one foot long and was located just down stream of the diaphragm. The addition of the cold trap has no noticable effect on the performance of the shock tube since the shock wave in this region is already seriously perturbed by the opening of the diaphragm.

The initial pressure in the test section was measured by a manometer or alphatron gauge with an estimated error of ±5%.

The shock speeds were measured in the Pyrex tube by observing the light emitted by the shock wave as it passed a series of 5 equally-spaced slits arranged along the last half of the shock tube. In the steel tube ionization pickups were employed to detect the passage of the shock. The outputs of the speed pickups were displayed on a folded oscilloscope sweep which was normally read to the nearest microsecond. For pickup intervals of 30 cm this produced an error of ±0.7% in the speed measurement for a median shock speed of 4 mm/μsec. Shock speed histories for several typical shock waves in the 4.5 mm/μsec range are shown in Fig. 3a. The deceleration observed is characteristic of combustion-driven shock waves and constitutes one of the most difficult effects to account for in the interpretation of the data.

CHARACTERISTICS OF INCIDENT SHOCK WAVES

Figure 4 shows a time-resolved photograph of a shock wave moving past a 1-mm slit perpendicular to the shock tube axis. The photograph was made with an $f/2$ pneumatically driven drum camera at a film speed of 0.08 mm/μsec. Also shown in the figure is an x–t diagram of the shock wave and two schematic views of the shock tube illustrating the slit arrangement.

The luminosity jumps abruptly at the shock front and remains roughly constant for approximately 30 μsec. Following this the luminosity becomes erratic due to the arrival of the turbulent mixed zone ahead of the relatively cold driver gases. There is no evidence of important boundary layer radiation in the photograph. Note that light from the gas may be distinguished from light from the boundary layer by the fact that, for a tube of a circular cross section, the former produces maximum intensity across the center of the tube while the latter produces intensity maxima along the walls. These effects can be clearly seen in the densitometer recordings shown at the bottom of Fig. 4.

In the past, the presence of a highly luminous boundary layer along the shock tube wall has caused considerable confusion in the interpretation of optical and spectroscopic studies made in shock tubes. In stainless steel tubes the boundary layer radiation dominates the gas radiation. Even in new Pyrex tubes the bound-

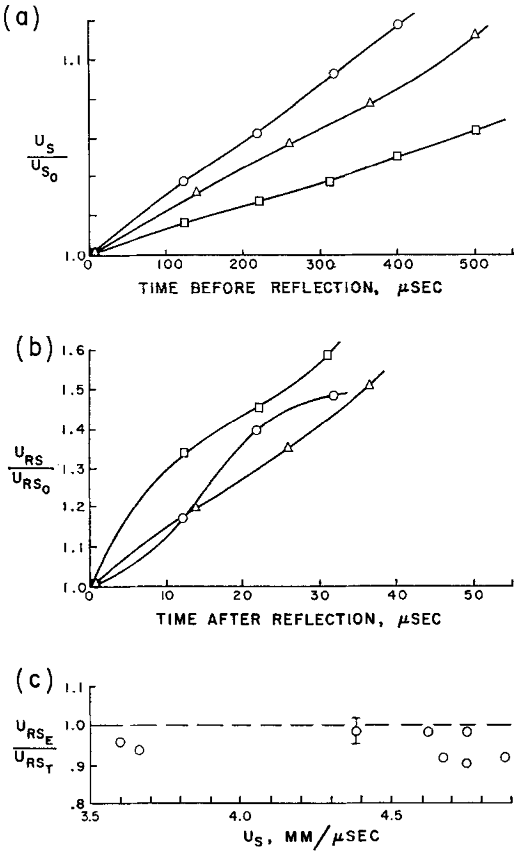

FIG. 3. Parts (a) and (b) show normalized shock speed histories for several typical shock waves before and after reflection; like symbols refer to the same run. Part (c) shows the ratio of the experimental to theoretical reflected shock speed for a number of typical runs including those shown in parts (a) and (b).

ary layer dominates the radiation. However, with repeated running a Pyrex tube may be "cleaned up" as shown by Fig. 4. Although this solves the problem of the emission from the boundary layer, its effect in absorption must still be considered in radiation problems.

CHARACTERISTICS OF REFLECTED SHOCK WAVES

The reflection of a shock wave gives rise to some interesting gas dynamic phenomena which have proved troublesome in the present experiment. The first of these is the growth of "feet" on the reflected shock wave. These "feet" have been studied extensively by Mark (*21*) using schlieren techniques and have been interpreted by him as due to an interaction between the reflected shock wave and

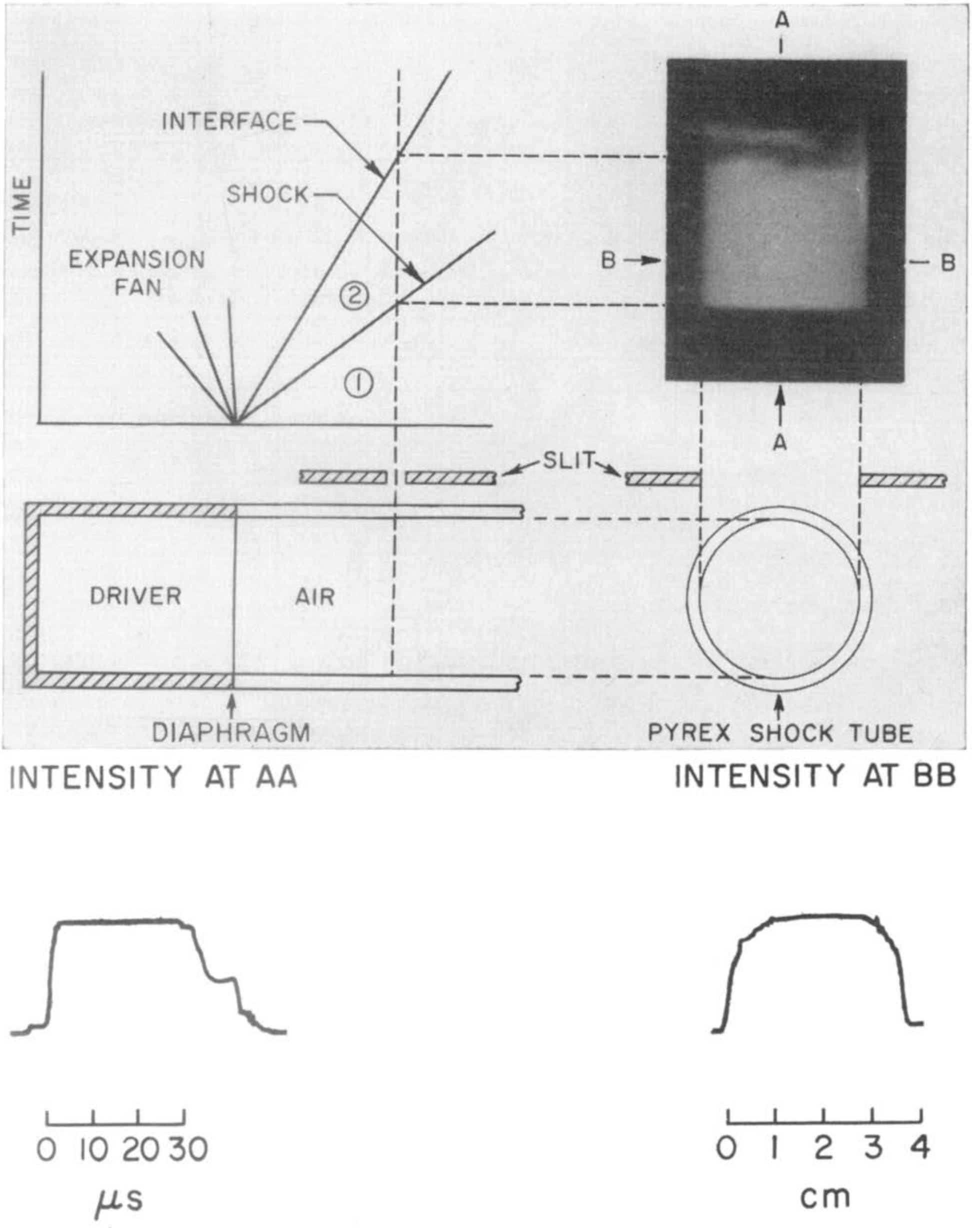

FIG. 4. Time-resolved photograph of a typical shock wave moving past a slit perpendicular to the shock tube axis. The position of the slit, the shock tube and an x–t diagram are shown schematically. Also shown are densitometer traces of the photograph illustrating the intensity variation both parallel and perpendicular to the shock tube axis.

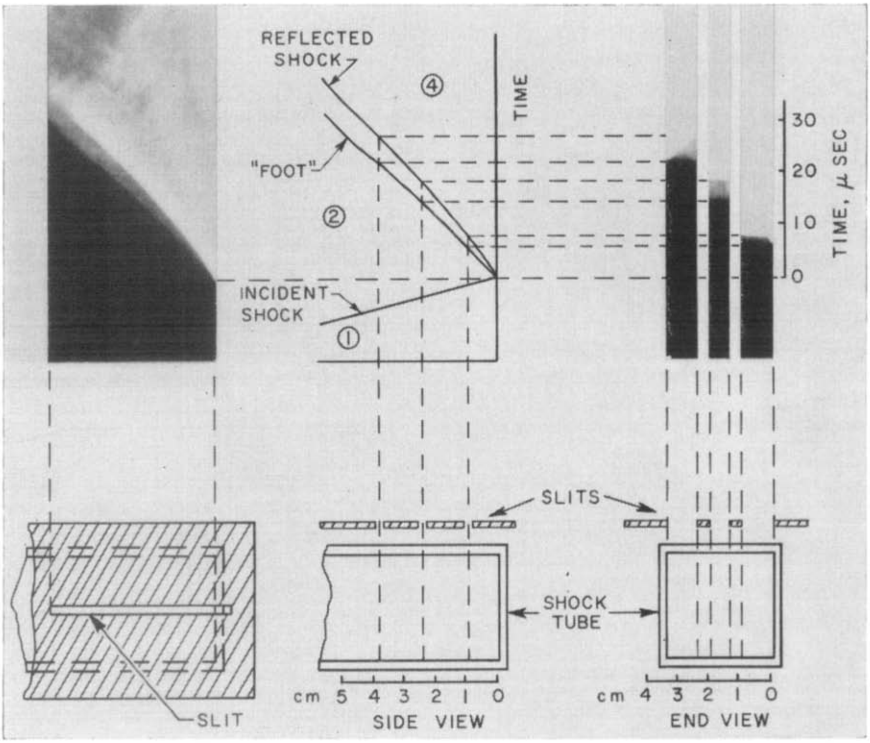

FIG. 5. Time-resolved photograph of a typical shock wave moving past horizontal and vertical slits illustrating the acceleration of the reflected shock wave and the growth of the "foot" discussed in the text.

the boundary layer behind the incident shock wave. They are clearly visible in time-resolved photographs taken by the slit method described above and are shown in Fig. 5. The geometry may be reconstructed by reference to the x–t diagram and the schematic drawings of the shock tube. It will be noted that this particular set of photographs was taken using a square shock tube.

The presence of such large "feet" on the reflected shock wave implies nonuniformities in the flow behind the reflected shock wave which could have important effects on photometric and spectroscopic studies made transverse to the shock tube. There is some evidence of this in Fig. 5, which shows that the luminosity behind the reflected shock wave is nonuniform. In addition, spectrographic studies discussed in Section III show heavy contamination with impurities. Largely for these reasons the observations on reflected shock waves were made looking along the tube axis.

A second troublesome phenomenon which is seen clearly in Fig. 5 is the acceleration of the reflected shock wave. Several speed histories for reflected shock waves derived from photographs similar to that shown in Fig. 5 are shown in Fig. 3b. Although the percent acceleration is relatively large, the effect on the enthalpy of the gas behind the shock wave is small due to the relatively high enthalpy of the incident stream. The acceleration has been studied by Rose and Nelson (*22*) who associate it with the decleration of the incident shock wave. It is not well understood, however, and constitutes a major uncertainty in the interpretation of the data.

The ratio of the measured initial reflected shock speed to that predicted theoretically from the measured incident shock speed at the time of reflection is shown in Fig. 3c. The vertical bar shows the estimated random error in the measurement of an individual point. In addition, there is a systematic error of about the same magnitude due to an uncertainty of $\pm 1°$ in the alignment of the shock tube axis and the axis of rotation of the drum camera. Although the average of the points indicates that the measured reflected shock velocity is slightly low, the discrepancy is within that attributable to alignment errors and is not considered significant. This suggests that if we measure the incident shock velocity at the time of reflection and confine our observations on the reflected shock to a short interval thereafter we should be fairly safe in using the theory to calculate temperatures and densities.

CALCULATION OF SHOCK CONDITIONS

The temperature and density behind shock waves in air were deduced from the measured initial density and shock speed using the curves in Feldman's "Hypersonic Gas Dynamic Charts for Equilibrium Air." (*23*) The equilibrium concentrations of the various atomic and molecular species were calculated by Teare at the Avco Research Laboratory directly from their partition functions and checked against both the Rand (*24*) and the Cornell Aeronautical Laboratory (*25*) tables. Conditions behind shock waves in O_2 and N_2 were calculated by Teare.

The main uncertainty in using shock wave theory to deduce the gas conditions centers on the range of validity of the equilibrium assumptions. This has been the subject of intensive study at the Avco Research Laboratory and will be dealt with at intervals throughout this report. In general, the conclusion is that the equilibrium assumption is valid for the conditions of the present experiments.

II. SPECTROGRAPHIC STUDIES

Photographic studies of the spectra produced by reflected shock waves in oxygen, nitrogen and air (21% O_2 + 79% N_2) were made to determine the qualitative features of the radiation. Two spectrographs were employed: one was

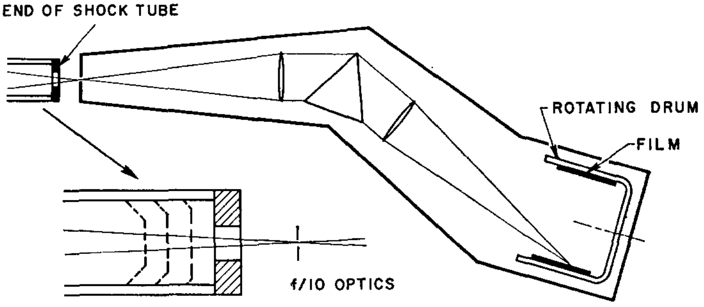

FIG. 6. Schematic of drum camera spectrograph in position to make axial spectrograms of reflected shock waves. The blow-up shows that this geometry avoids photographic radiation from the "foot"; the dashed lines show the reflected shock wave and "foot" at 10 μsec intervals.

equipped with a moving film on which a complete time history of the radiation could be obtained, and the other was equipped with a shutter which could be triggered to give exposures down to 10 μsec. The quality of the spectra obtained with the latter system was superior to that obtained with the former, and it was used when detail was desired. The former system was used in preliminary surveys of the general characteristics of the radiation to obtain information concerning the proper timing of the shutter and the most favorable geometry in which to set up the spectrograph.

Drum Camera Spectra

A preliminary study of the radiation produced by reflected shock waves was made using the drum camera spectrograph shown schematically in Fig. 6. Spectra were obtained for two directions of observation: one looking across the shock tube through a window 0.5 cm from the closed end of the shock tube and the other looking along the axis of the tube through a window in the end plate. The spectra are shown in Fig. 7. Note that the axial view shows an interval of about 30 μsec during which the spectrum is relatively free of radiation from impurities while the transverse view shows strong radiation from impurities starting the moment the shock wave passes the observation station. This situation indicates that both the boundary layer along the shock tube wall and the turbulent mixed zone ahead of the driver are heavily contaminated by material picked up at the shock tube walls, but there is a region of clean gas along the shock tube axis on which observations may be made for about 30 μsec looking through the end of the tube. Even this region shows some radiation from impurities (notably CN) which can be associated with the vapor pressure or organic compounds which have not been pumped out of the tube. The partial pressure of these impurities is not as serious as might be thought from the prominence of CN in the spectrum,

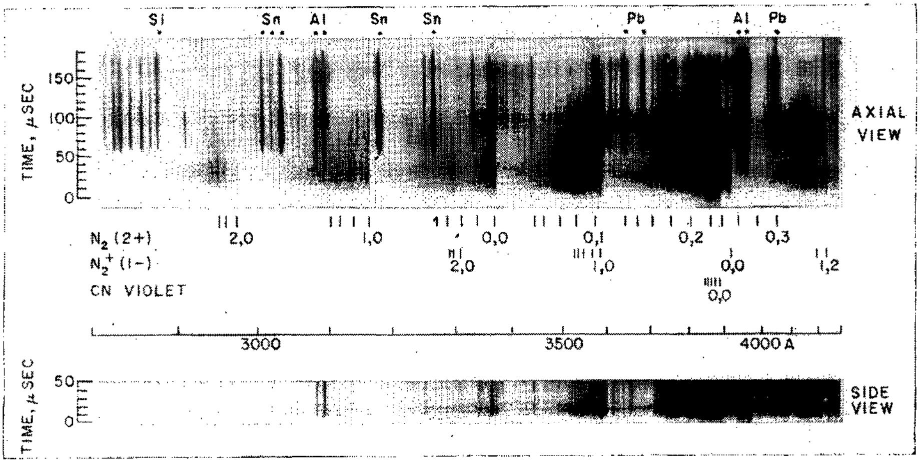

FIG. 7. Time-resolved spectrograms of air heated by reflected shock waves taken with the drum camera. Both axial and side views are shown; the side viewing position was 0.5 cm from the end of the tube. Note that the spectrum observed axially is relatively free of radiation from impurities for approximately 30 μsec while strong radiation from impurities appears immediately in the side view. These impurities are associated with the boundary layer.

however. The CN violet band system is an extraordinarily prominent source of radiation due to a relatively large *f*-number of order 0.1, the narrowness of the bands because of the similarity of its electronic potentials, and the fact that the radiation comes from a low-lying upper state. Less than one part-per-million of CN is sufficient to produce the intensity observed in the spectra shown. By employing a Pyrex tube (which shattered on every run with reflected shock waves) and a liquid N_2 trap it was possible to virtually eliminate CN from the spectrum. Such extreme measures were not normally employed since the presence of a small CN impurity did not appear to affect the radiation from other sources.

SHUTTERED SPECTRA

As a result of the observations made with the drum camera, it appeared that the cleanest spectra could be obtained by looking along the shock tube axis and recording the radiation within the first 30 μsec after reflection of the shock wave. The spectrograph used was an *f*/10 Hilger having interchangeable glass and quartz optics and an electromechanical shutter designed by Camm (*26*). This shutter had a characteristic delay of 25 ± 5 μsec and operated at exposure times down to 10 μsec. In normal operation the shutter was set to open 5 μsec before and close 20 μsec after reflection of the shock wave. It was not satisfactory to start with the shutter open and simply close it since the integrated exposure from

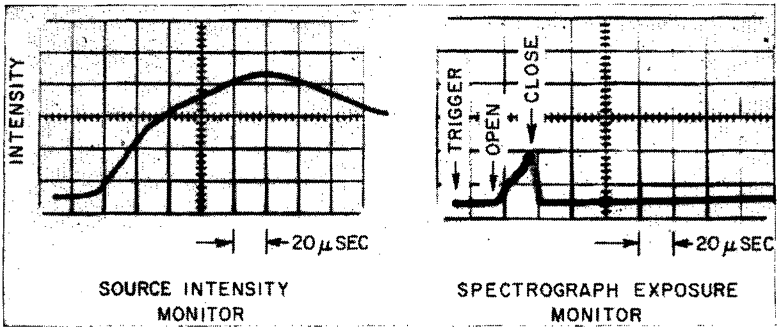

FIG. 8. Phototube traces illustrating the operation of the spectrograph shutter. Impurity radiation which appears after 30 μsec, as shown in Fig. 7, is avoided by closing the shutter 20 μsec after reflection of the shock wave.

the oncoming incident shock was of the order of that from the reflected shock. The performance of the shutter was monitored by a phototube which picked up a portion of the light entering the spectrograph. The output of this phototube compared with that of an unshuttered phototube looking at the same shock as shown in Fig. 8. A useful feature of the shutter is that with it one can superimpose the spectra of several shocks to obtain increased exposure. This was done in studying the radiation from the N_2 first positive band system in nitrogen.

The emission spectra of oxygen, nitrogen, and air (21% O_2 + 79% N_2) obtained with the shuttered spectrograph are shown in Fig. 9. The conditions under which these were obtained are given in the figure caption.

Molecular bands which are easily identified include O_2 Schumann-Runge, NO

FIG. 9. Shock tube spectra of air, oxygen, and nitrogen. All spectrograms were taken with an *f*/10 Hilger spectrograph with a 40-micron slit width. Spectrograms (a), (b), and (c) were made with quartz optics; (d), (e), and (f) with glass. Exposure times were about 20 μsec, the electromechanical shutter opening about 5 microseconds before shock reflection and closing about 20 μsec after reflection. The average thickness of the gas source was about 1 cm. The spectrograms were broadened by moving the paper during printing. Details pertaining to the individual spectrograms are tabulated below.

Spectrum	Gas	Temperature (°K)	Density (ρ_0)	Spectral region (Angstroms)	Plate type Kodak
(a)	Air	8100	0.83	2200–5000	103–O
(b)	N_2	8200	0.79	2200–5000	103–O
(c)	O_2	6100	1.13	2200–5000	103–O
(d)	Air	8500	0.88	3700–7000	103-F
(e)	N_2	8700	0.90	3700–7000	103-F
		8200	0.79	7000–9000	1–N
(f)	O_2	10400	0.50	3700–4900	1–N
		11800	0.48	4900–7000	103–F
		10400	0.50	7000–9000	1–N

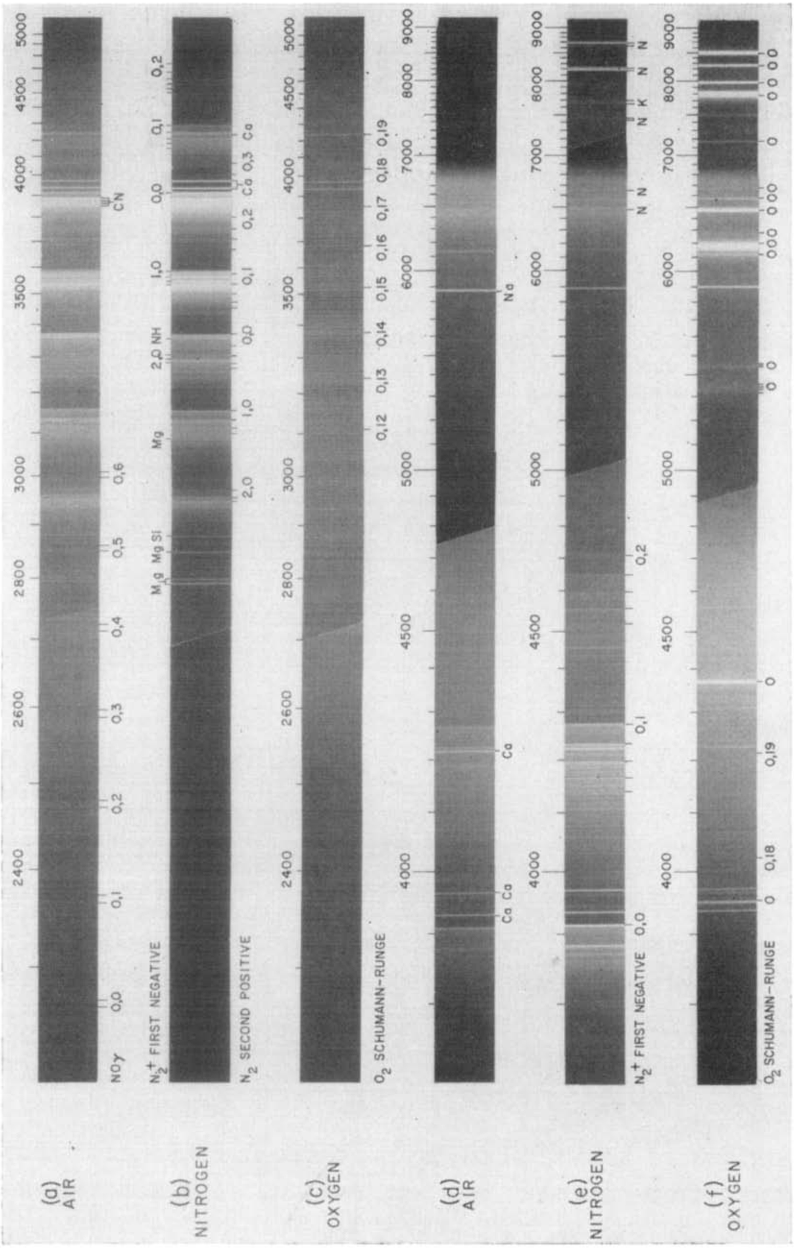
(a) AIR
NOγ
0,0
0,1
0,2
0,3
0,4
0,5
0,6
CN
(b) NITROGEN
N_2^+ FIRST NEGATIVE
N_2 SECOND POSITIVE
Mg
Mg Si
Mg
NH
Ca
(c) OXYGEN
O_2 SCHUMANN-RUNGE
0,12
0,13
0,14
0,15
0,16
0,17
0,18
0,19
(d) AIR
Ca Ca
Ca
Na
(e) NITROGEN
N_2^+ FIRST NEGATIVE
N
K
(f) OXYGEN
O_2 SCHUMANN-RUNGE
O
2400
2600
2800
3000
3500
4000
4500
5000
6000
7000
8000
9000

Fig. 9.

γ, N_2 second positive and N_2^+ first negative. No structure definitely associated with the NO β bands can be seen in the spectra but it is quite clear that NO γ bands are superimposed on background radiation which it is logical to ascribe to the NO β bands. In addition the general distribution of the radiation in the near infrared is similar to that of the N_2 first positive bands. This is shown in more detail by the densitometer records in Fig. 10.

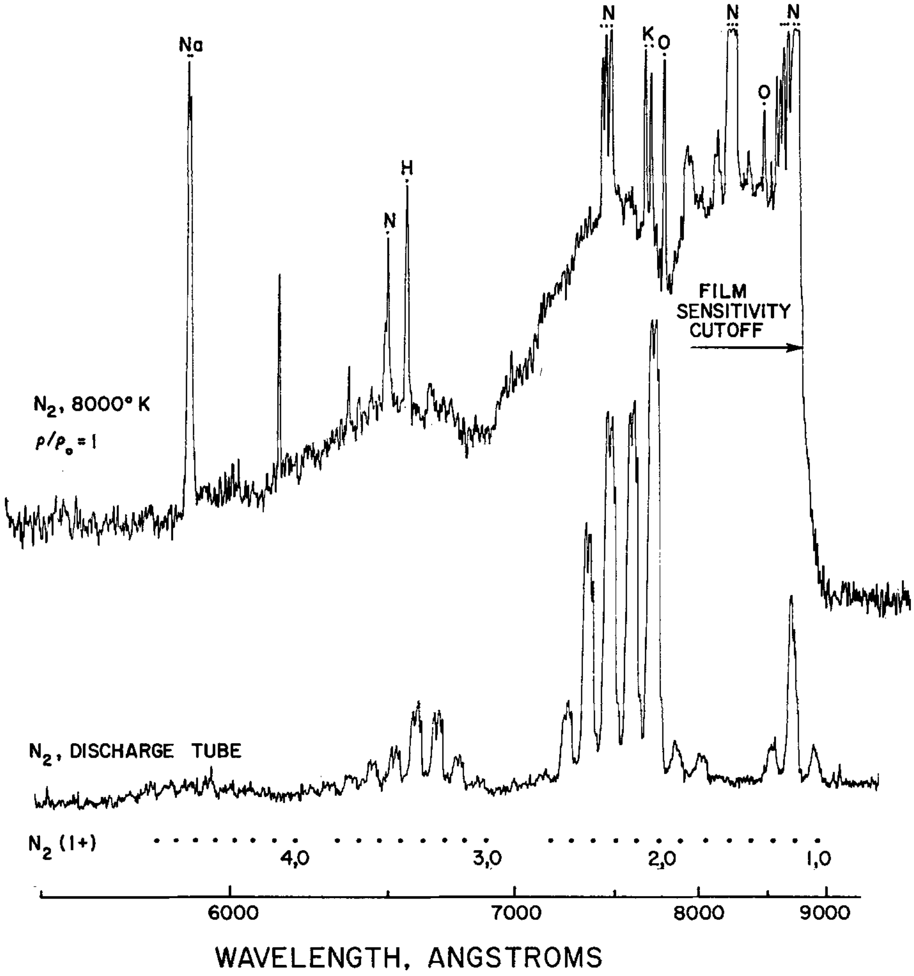

FIG. 10. Densitometer traces of spectrograms comparing the radiation from nitrogen heated by a reflected shock wave with that from nitrogen in a discharge tube. Although positive identification of individual band heads is difficult in the shock tube spectrum due to strong overlapping of rotational structure, the general similarity of the two traces indicates that a major part of the shock tube radiation in this wavelength region is due to the N_2 first positive bands.

TABLE I

WAVELENGTHS OF O AND N LINES OBSERVED IN THE SHOCK TUBE SPECTRUM OF AIR AT 8000°K AND NORMAL DENSITY

Nitrogen			Oxygen
6483[a]	8185[a]	8568	7948[a]
6484[a]	8188[a]	8594	7951[a]
6485[a]	8201[a]	8630	7952[a]
6645	8211[a]	8680[a]	8446[a]
7424	8216[a]	8684[a]	8447[a]
7443	8223[a]	8686[a]	
7469	8243	8712[a]	
		8719[a]	

[a] Unresolved.

There is also evidence of continuum radiation in the visible region of the spectrum. This is interpreted as Kramers radiation from O^- and the intensity is consistent with that which can be deduced by detailed balancing arguments from the photodetachment cross section of Branscomb *et al.* (*27*).

A number of atomic lines from both O and N were observed in the spectra. Their wavelengths are tabulated in Table I.

III. PHOTOMETRIC STUDIES

Measurements of the absolute spectral intensity of the radiation from air and oxygen were made using a grating monochromator and calibrated phototubes. The experimental apparatus is shown schematically in Fig. 11. The luminous gas was imaged at the entrance slit of the monochromator by an optical train consisting of two aluminized mirrors. For measurements on incident shock waves the monochromator was equipped with two Dumont 6292 photomultipliers: one which measured the intensity in a narrow wavelength band selected by the monochromator, and a second which monitored a fraction of the light passing through the entrance slit and provided an indirect check on the measured shock speed. For reflected shock waves the photomultipliers were replaced by 935 photocells for measurements in the violet wavelength region and 917 photocells for measurements in the red.

The outputs of the phototubes were fed either directly or via cathode followers to Tektronix oscilloscopes having rise-times of 0.3 μsec or better. The traces were photographed using Land cameras.

CALIBRATION

Overall calibration of the complete optical train including shock tube windows and appropriate filters to prevent overlapping of orders was made using both a standard tungsten ribbon filament lamp and a graphite arc.

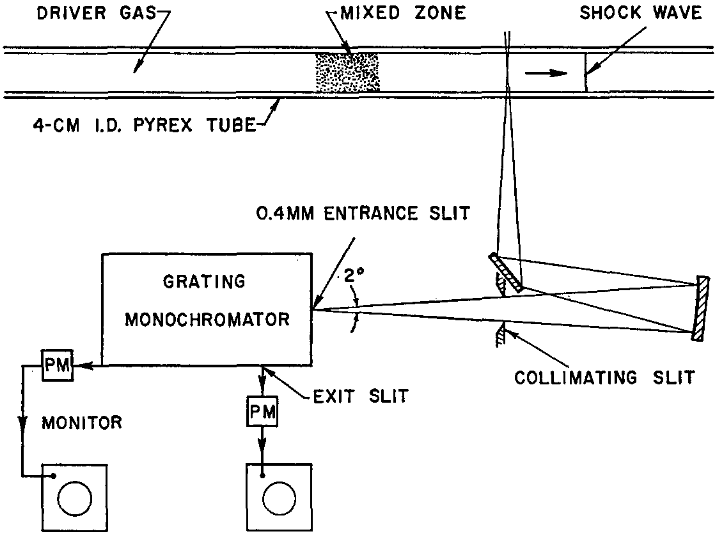

FIG. 11. Schematic diagram of monochromator in position to record radiation from shock waves.

The brightness temperature of the standard lamp was given as a function of lamp current at a wavelength of 6530A by the National Bureau of Standards. The spectral intensity of the lamp at other wavelengths was calculated using data on the emissivity of tungsten given by DeVos (*28*) and the measured transmission characteristics of the quartz window. The standard lamp was used to calibrate from 3500 to 10,000A.

To obtain a calibration at shorter wavelengths a graphite arc was used. Data on the true temperature and spectral emissivity of such arcs has been given by Euler (*29*). They are roughly gray bodies having a true temperature of 4000°K and an emissivity of 0.75. A check on the brightness temperature of the arc which agreed with Euler's value with 15°K was made using a Leeds and Northrup optical pyrometer. The graphite arc was used to calibrate from 2500 to 10,000A. In the region of overlap the two methods of calibration agreed with each other within 20% or better. This was regarded as satisfactory for the present purposes since fluctuations in shock tube operation produced variations of this order.

INCIDENT SHOCK WAVE MEASUREMENTS

Typical traces of the radiation from air as a function of time after the passage of both "fast" and "slow" shock waves are shown in Fig. 12.

For the "slow" shock wave the radiation rises monotonically to a steady state value in a time of the order of 5 μsec. The noise on the trace is due to statistical

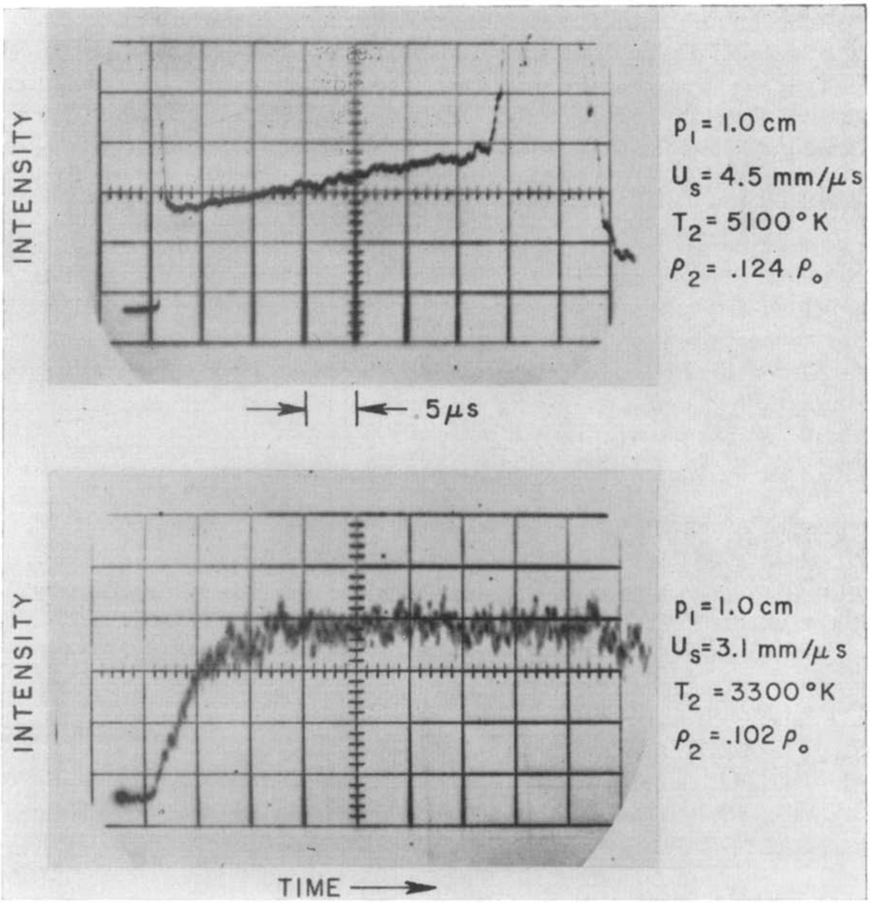

FIG. 12. Intensity histories recorded by the monochromator monitor for "fast" (u_s = 4.5 mm/µsec) and "slow" (u_s = 3.1 mm/µsec) speed shock waves. The radiation was observed looking across the shock tube as shown in Fig. 11. The ordinates for the two traces are not to the same scale.

fluctuations in the number of photons counted within the resolving time of the electronics. The uniformity of the steady state signal attests to the uniformity of hydrogen-driven shocks. In the analysis of the data the steady state level was assumed to be the equilibrium level.

For the "fast" shock wave the radiation at the shock front goes through a maximum before approaching a relatively steady value. This maximum has been shown spectrographically to be largely due to radiation from the first negative bands of N_2^+ in the high temperature relaxation zone following the shock front.

Following the maximum the radiation falls, then rises slowly for an interval of approximately 35 μsec, after which it becomes erratic indicating the arrival of the mixed zone preceding the driver gas. The slow rise mentioned above is characteristic of uniformly decelerating shock waves and is interpreted as due to an increase in the temperature with distance behind the shock front. The percentage variation in intensity is roughly three times the percentage variation in shock speed. As will be seen later, the percentage change in the initial amplitude of the equilibrium radiation is roughly 10 times the percentage change in the instantaneous shock speed, showing that considerable smoothing of conditions occurs behind decelerating shock waves due to the propagation of sound waves. It might be mentioned that in the case of accelerating shock waves the radiation is observed to fall with time as expected. In the analysis of nonuniform shock waves the radiation was extrapolated to the shock front and correlated with the instantaneous shock speed.

REFLECTED SHOCK MEASUREMENTS

Observations on reflected shock waves were made looking along the shock tube axis through a quartz window in the end of the tube. Typical traces of the radiation from air as a function of time after the reflection of both "fast" and "slow" shock waves are shown in Fig. 13. The incident shock conditions correspond very closely to those for the incident shock waves shown in Fig. 12. The difference between the "fast" and "slow" traces is negligible. Apart from small-amplitude oscillations, both traces rise linearly with time as the thickness of the radiating layer increases. No radiation is observed prior to reflection of the shock wave due to the fact that the specific brightness of the incident shock wave is only 10^{-3} that of the reflected shock wave. After about 35 μsec the "fast" shock wave encounters the mixed zone and the radiation becomes erratic; the "slow" shock wave has not yet encountered the mixed zone at the end of the trace. In view of the pronounced accelerations which were observed for "fast" reflected shock waves it is somewhat surprising to note that the rise in the intensity of the light emitted is so nearly linear. Apparently, some sort of canceling effects must be occurring which are not at present understood.

In the analysis of the reflected shock data the intensity of the radiation per centimeter thickness of gas was determined by dividing the mean rate of rise of intensity for the first 15 μsec after reflection by the reflected shock velocity at the time of reflection. This was the closest practical approach which could be made to the objective of measuring the radiation at the time of reflection as a means of circumventing the problem of the accelerating reflected shock.

EXPERIMENTAL RESULTS

The spectral intensity of the equilibrium radiation from oxygen and air (21% O_2 + 79% N_2) heated by incident shock waves is shown as a function of wave-

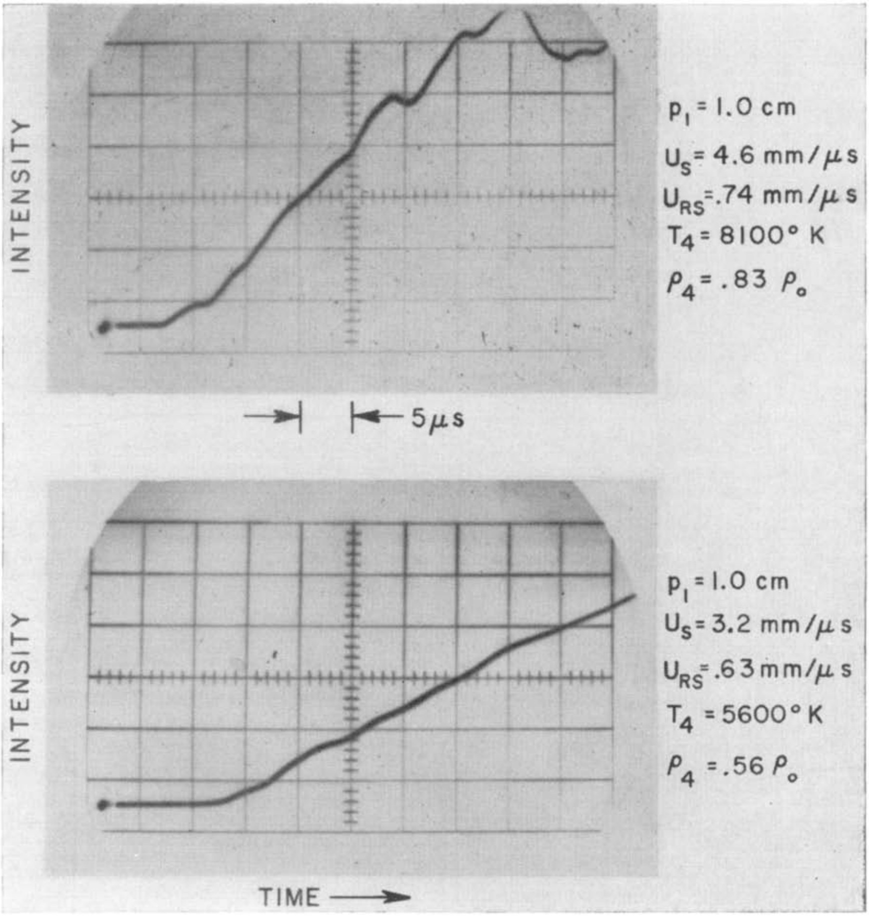

FIG. 13. Intensity histories for reflected shock waves recorded by the monochromator monitor for reflected shock waves viewed axial. The incident shock conditions correspond closely to those for the shock waves in Fig. 12. The ordinates for the two traces are not to the same scale.

length and shock speed in Figs. 14 and 15. The intensity of the radiation from air (21 % O_2 + 79 % N_2) heated by reflected shock waves is shown as a function of shock speed, density, and wavelength in Figs. 16–18. The curves in Figs. 14–18 represent a reconstruction of the radiation based on the theory given in the following section.

On the intensity versus shock speed graphs the experimental points are plotted directly. In the other cases it was, in general, necessary to interpolate or extrapolate the data to a fixed shock speed because the speed of an individual shock

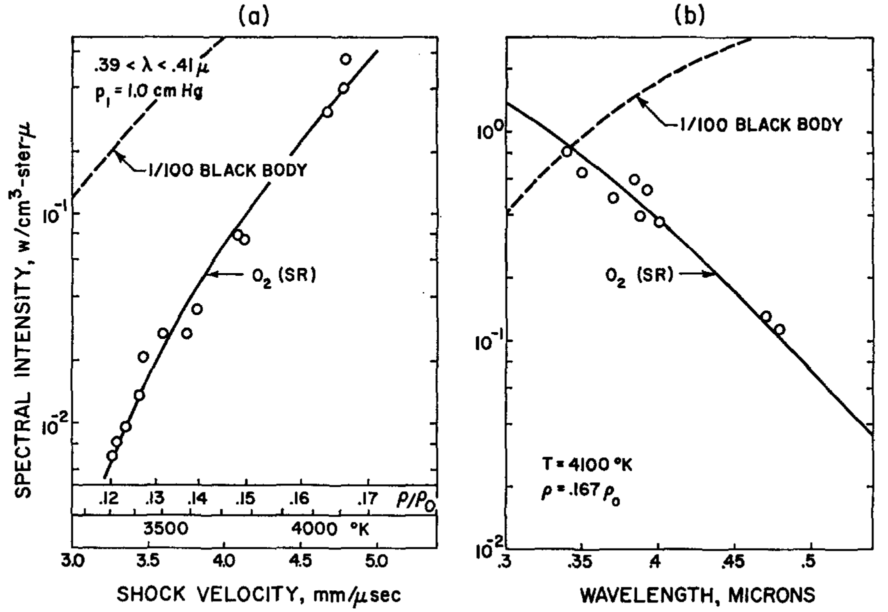

FIG. 14. Spectral intensity of the radiation from shock heated oxygen as a function of shock velocity and wavelength. The measurements were made looking across the 1.5-inch Pyrex shock tube. The curves were reconstructed from the theory given in the text.

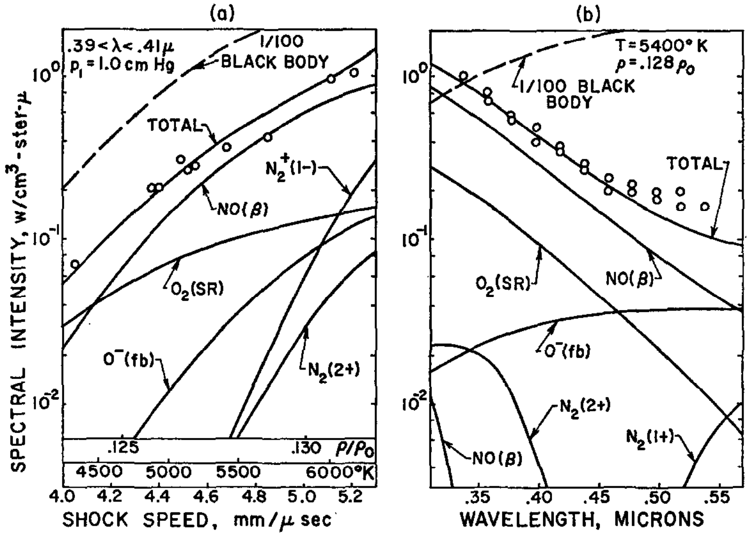

FIG. 15. Spectral intensity of the radiation from shock heated air (21% O_2 + 79% N_2) as a function of shock speed and wavelength. The measurements were made looking across the 1.5-inch Pyrex shock tube. The curves were reconstructed from the theory given in the text.

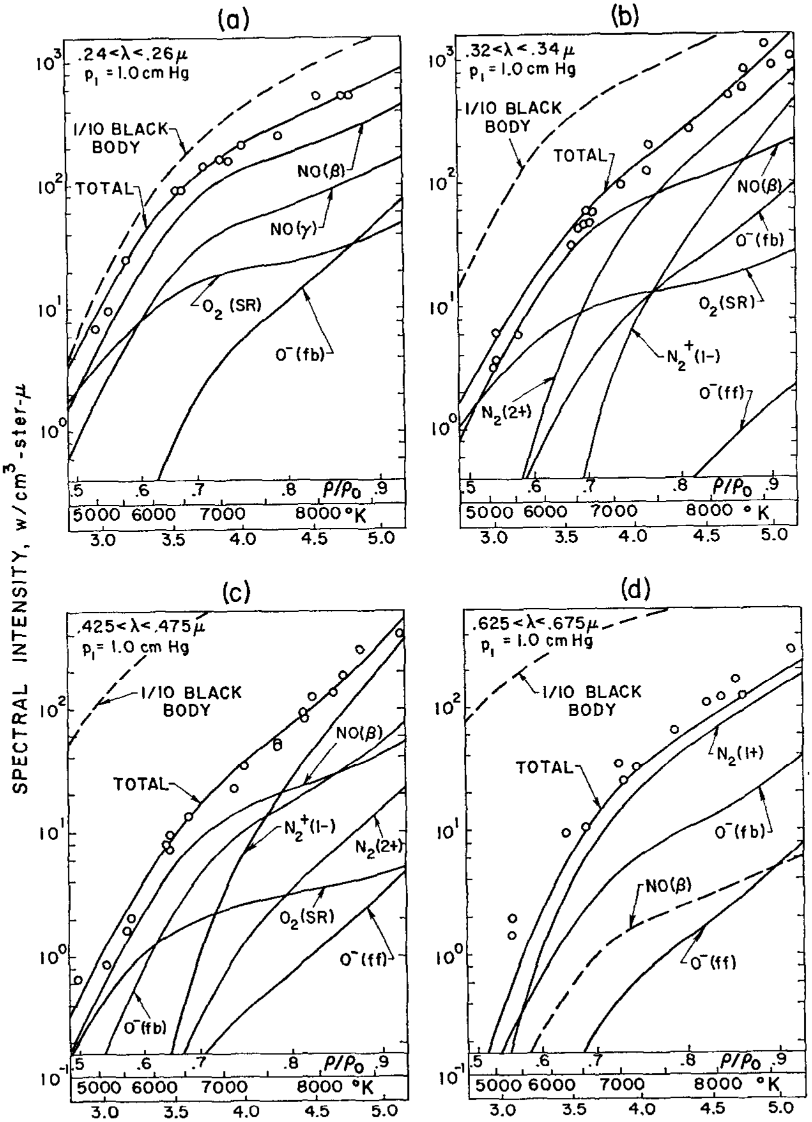

FIG. 16. Spectral intensity of the radiation from air (21% O_2 + 79% N_2) heated by reflected shock waves as a function of the incident shock speed for four wavelength intervals. The measurements were made looking along the tube axis and the effective sample thickness was approximately 1.0 cm. The curves were reconstructed from the theory given in the text.

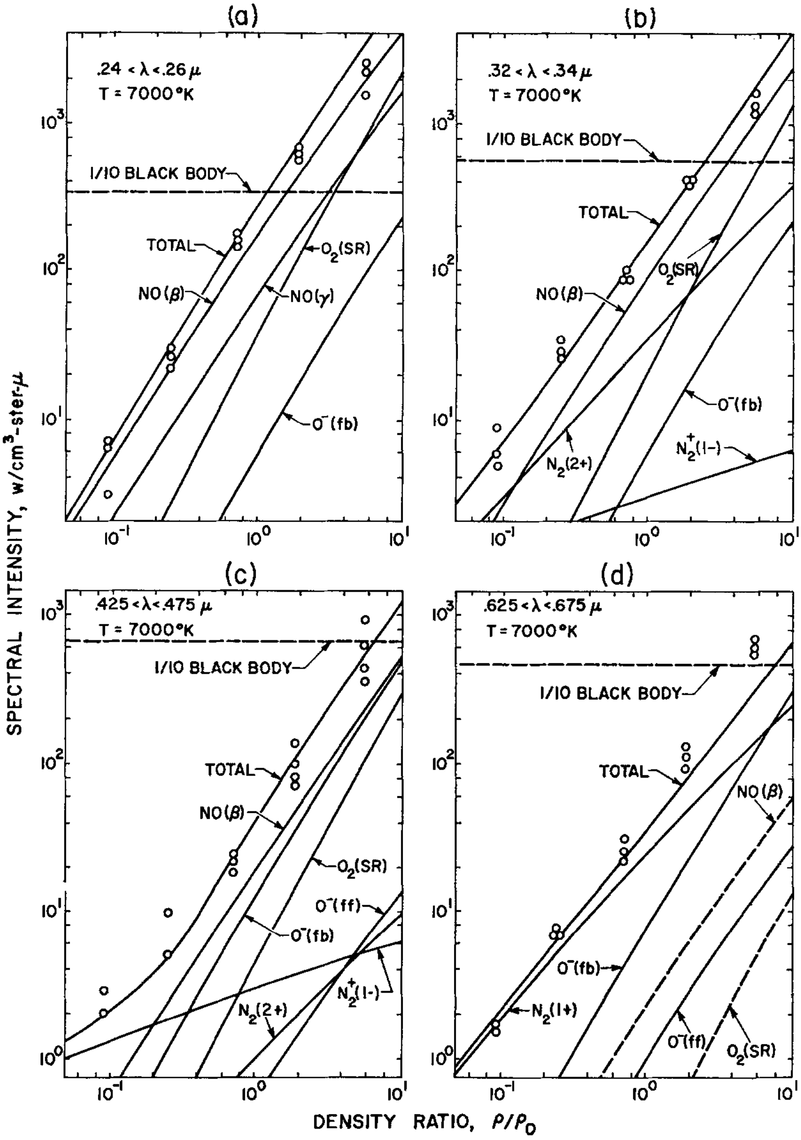

FIG. 17. Spectral intensity of the radiation from air (21% O_2 + 79% N_2) heated by reflected shock waves as a function of density for four wavelength intervals. The measurements were made looking along the tube axis and the effective sample thickness was approximately 1.0 cm. The curves were reconstructed from the theory given in the text.

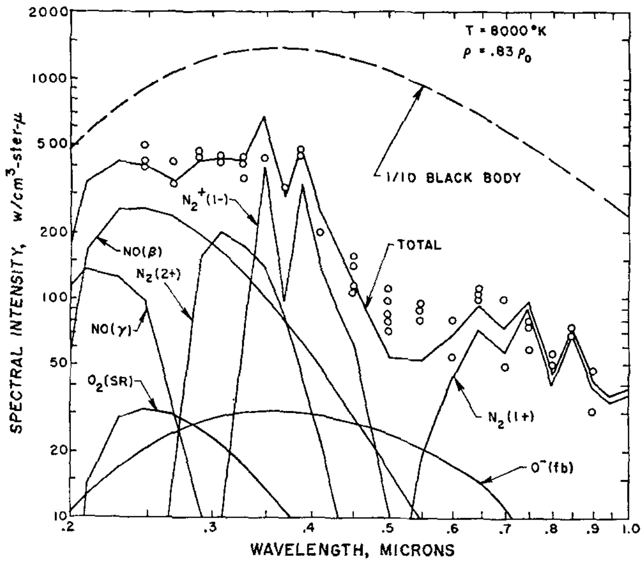

FIG. 18. Spectral intensity of the radiation from air (21% O_2 + 79% N_2) heated by reflected shock waves as a function of wavelength. The measurements were made looking along the tube axis and the effective sample thickness was approximately 1.0 cm. The curves were reconstructed from the theory given in the text.

wave could only be predicted in advance with an error of about 5%. The variation of intensity with shock speed given by the theory was used as a guide in this process.

IV. ANALYSIS OF DATA

The problem of relating the average emission of a molecular band to the electronic f-number has been treated by Meyerott (*5*) and by Kivel *et al.* (*4*) (KMB). Their results may be summarized as follows:

For a slab of gas of thickness, l, in which the molecules are in thermodynamic equilibrium at a temperature, T, the radiation per unit area in the wavelength interval λ to $\lambda + d\lambda$ into a solid angle $d\Omega$ normal to the layer is:

$$\frac{dI}{dA\,d\Omega\,d\lambda} = (1 - e^{-\mu_\lambda' l}) \frac{dB}{dA\,d\Omega\,d\lambda}, \tag{1}$$

where

$$\frac{dB}{dA\,d\Omega\,d\lambda} = 2hc^2\lambda^{-5}(e^{hc/kT\lambda} - 1)^{-1} \tag{2}$$

is the black body intensity, and

$$\mu_\lambda' = \mu_\lambda(1 - e^{-hc/kT\lambda}) \tag{3}$$

is the apparent absorption coefficient. μ_λ' differs from the true absorption coefficient, μ_λ, by the factor in parenthesis which corrects for induced emission. In the special case of an optically thin gas layer, i.e., $\mu_\lambda' l \ll 1$, Eqs. (1–3) may be combined in the form:

$$\frac{dI}{dA\,d\Omega\,d\lambda} \doteq \mu_\lambda l \cdot 2hc^2\lambda^{-5}e^{-hc/kT\lambda}. \tag{4}$$

Thus, a measurement of the spectral brightness of an optically thin gas in thermodynamic equilibrium may be used to determine the true absorption coefficient, μ_λ.

For a molecule, μ_λ is a complicated sum over many overlapping lines which when averaged with respect to rotational structure may be written:

$$\mu_\lambda = \pi r_0 f[X]\varphi \frac{hc}{kT} \exp\left[-\frac{hc}{kT}\left(\frac{1}{\lambda_{00}} - \frac{1}{\lambda}\right)\right], \tag{5}$$

where: $r_0 = e^2/mc^2$ is the classical electron radius,

$f = 8\pi^2 mc/3h\lambda \mid R \mid^2$ is the electronic f-number and the matrix element is a function of internuclear separation,

$[X]$ is the concentration and absorbing molecules, and

λ_{00} is the wavelength of the 0, 0 vibrational transition.

φ is a dimensionless factor of order unity which gives the details of the vibrational spectrum and is defined by the equation:

$$\varphi = \frac{kT}{hc} \cdot \frac{1}{Q_v'' Q_r'' (B_e' - B_e'')} \cdot \sum_{\epsilon_r' \geqq 0} q_{v'v''} e^{-(\epsilon_v' + \epsilon_r')/kT}, \tag{6}$$

where: $Q_v'' = [1 - \exp(-hc\omega_e''/kT)]^{-1}$ is the vibrational partition function for the absorbing state, (the $'$ refers to the excited electronic or emitting state and the $''$ refers to lower electronic or absorbing state);

$Q_r'' = kT/hcB_e''$ is the rotational partition function for the absorbing state;

$q_{v'v''}$ is the Condon factor for the transition from v' to v'';

$\epsilon_v' = hc(1/\lambda_{v'} - 1/\lambda_{0'})$ is the vibrational energy relative to the ground vibrational state for the emitting state;

$\epsilon_r' = B_e'/(B_e' - B_e'').\ hc(1/\lambda - 1/\lambda_{v'v''})$ is the rotational energy for the emitting state;

$1/\lambda_v = \omega_e(v + 1/2) - \omega_e x_e(v + 1/2)^2 + \omega_e y_e(v + 1/2)^3$ is the wave number of the vth vibrational level; and

$1/\lambda_{v'v''} = 1/\lambda_{00} + (1/\lambda_{v'} - 1/\lambda_{0'}) - (1/\lambda_{v''} - 1/\lambda_{0''})$ is the wave number for the vibrational transition between the states v' and v''.

The constants ω_e, $\omega_e x_e$, $\omega_e y_e$, B_e, and $\nu_{00} = 1/\lambda_{00}$ obtained from Herzberg's "Spectra of Diatomic Molecules" (*2*) are tabulated in Table II.

TABLE II

Spectroscopic Constants (*2*) for Molecular States Important in the Emission of Radiation from O_2, N_2, N_2^+, and NO

Molecule	State	ω_e cm^{-1}	$\omega_e x_e$ cm^{-1}	$\omega_e y_e$ cm^{-1}	B_e cm^{-1}	Transition	ν_{00} cm^{-1}	Band
O_2	$B^3\Sigma_u^-$	700.4	8.002	−0.375	0.819	$B \rightarrow X$	49363	Schumann-Runge
	$X^3\Sigma_g^-$	1580	12.07	0.0546	1.446			
N_2	$C^3\Pi_u$	2035	17.08	−2.15	1.826	$C \rightarrow B$	29670	Second positive
	$B^3\Pi_g$	1734	14.47		1.638	$B \rightarrow A$	9557	First positive
	$A^3\Sigma_u^+$	1460	13.89	−0.025	1.440	$A \rightarrow X$	49757	
	$X^1\Sigma_g^+$	2360	14.46	0.0075	2.010			
N_2^+	$B^2\Sigma_u^+$	2420	23.19	−0.538	2.083	$B \rightarrow X$	25566	First negative
	$X^2\Sigma_g^+$	2207	16.14	−0.040	1.932			
NO	$B^2\Pi$	1038	7.60	0.097	1.127	$B \rightarrow X$	45440	β bands
	$A^2\Sigma^+$	2371	14.48	−0.28	1.995	$A \rightarrow X$	44138	γ bands
	$X^2\Pi$	1904	13.97	−0.0012	1.705			

Note that the approximation discussed by KMB in Section II–E is equivalent to setting $\varphi \equiv 1$ and that in this approximation Eq. (5) of the present paper is identical with Eq. (2) of KMB.

Inserting Eq. (5) into Eq. (4) we obtain the following expression for the radiation from molecules of type X for $\mu_\lambda' l \ll 1$.

$$\frac{dI}{dA\,d\Omega\,d\lambda} \doteq \pi r_0 \cdot 2hc^2 \cdot f[X]l\varphi\lambda^{-5} \frac{hc}{kT} e^{-hc/kT\lambda_{00}}. \tag{7}$$

This equation is a slight generalization of Eq. (12) of KMB.

To compare the theoretical results with the experimental measurements, it is necessary to average Eq. (7) over the wavelength interval, $\Delta\lambda$, defined by the monochromator. The result for $\mu_\lambda' l \ll 1$ is:

$$\left\langle \frac{dI}{dA\,d\Omega\,d\lambda} \right\rangle_{\Delta\lambda} \doteq \pi r_0 \cdot 2hc^2 \cdot f[X]l\langle\varphi\rangle_{\Delta\lambda}\lambda^{-5} \frac{hc}{kT} e^{-hc/kT\lambda_{00}}, \tag{8}$$

where

$$\langle\varphi\rangle_{\Delta\lambda} = \frac{\lambda^6}{\Delta\lambda} \int_{\lambda-\Delta\lambda/2}^{\lambda+\Delta\lambda/2} \lambda'^{-6} \varphi\, d\lambda'.$$

Given the Condon factors and the basic spectroscopic data, it is a simple matter to compute $\langle\varphi\rangle_{\Delta\lambda}$ with the aid of a digital computer. The results for the most important molecular bands in air are plotted in Figs. 19–21, as a function of wavelength for several temperatures in the range 4000 to 10,000°K. The Condon factors used in the calculations for the N_2 first and second positive and N_2^+ first negative bands are those computed by Nicholls and co-workers (*30*). Those for the NO β and γ bands were taken from KMB. No sufficiently complete set of Condon factors was available for the O_2 Schumann–Runge bands and we have therefore computed them using an approximation discussed in Appendix I. The range of validity of our calculation of $\langle\varphi\rangle_{\Delta\lambda}$ is determined by the size of the table of Condon factors used. The summation in Eq. (6) converges because the factor $e^{-\epsilon_v'/kT}$ becomes small as the vibrational energy of the upper state, ϵ_v', be-

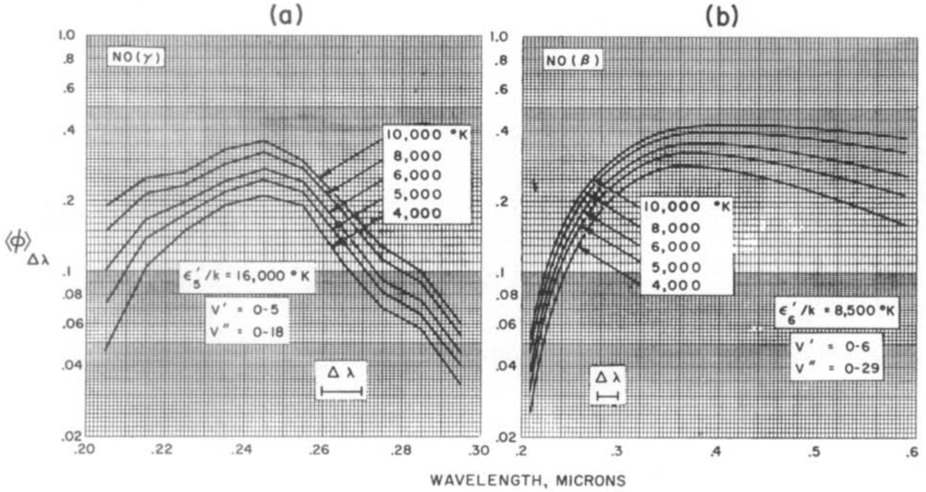

FIG. 19. Theoretical distribution functions used in computing the radiation from the NO γ and NO β bands.

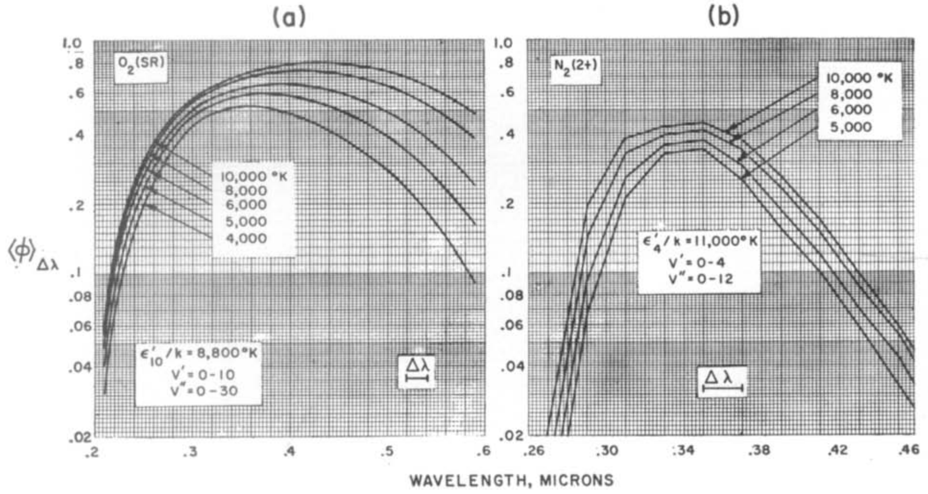

FIG. 20. Theoretical distribution functions used in computing the radiation from the O_2 Schumann–Runge and N_2 second positive bands.

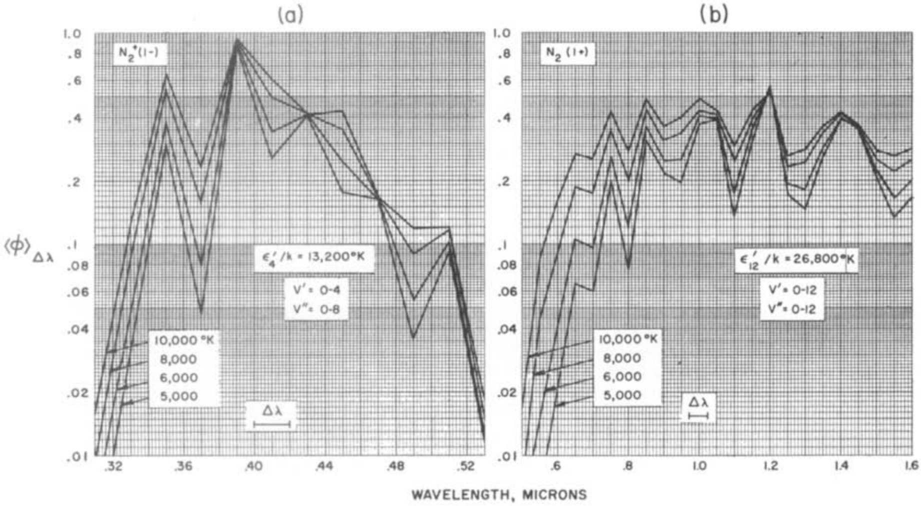

FIG. 21. Theoretical distribution functions used in computing the radiation from the N_2^+ first negative and N_2 first positive bands.

comes large. Thus our table must include entries for sufficiently large value of v' to make $kT \ll \epsilon_v'$. As can be seen from the values of $\epsilon_{v\max}'$ given in Figs. 19–21 this criterion was not well satisfied for the higher temperatures. It is nevertheless felt that the uncertainty in $\langle\varphi\rangle_{\Delta\lambda}$ is probably less than the uncertainty in the experimental results and is therefore of little practical importance for the present applications.

CALCULATION OF ELECTRONIC *f*-NUMBERS

If the shock-heated gas is assumed to be in thermodynamic equilibrium Eq. (8) may be used to compute the unknown *f*-numbers from the experimentally observed radiation intensities. In doing this we must bear in mind the restriction that the gas must be optically thin *everywhere*. Since the spectrum is composed of a series of lines, a rough criterion for this is that the observed emissivity, ϵ_λ, must be small compared to the ratio of mean line width, w, to mean line spacing, s. That is:

$$\epsilon_\lambda s/w \ll 1.$$

Values of s/w have been estimated by Meyerott and KMB. Their work shows that self-absorption for molecular band systems is generally not important at high temperatures as long as the average emissivity is less than 10%. This is because of the many vibration bands, each with many excited rotational lines, and the sufficiently broad Doppler width. The Doppler width provides a definitive and reasonable lower limit to the line width. Of course, at the higher gas densities collisions increase the line width and decrease any effect of self-absorption.

An experimental check that the gas is optically thin may be obtained by observing the dependence of the intensity on the density and thickness of the radiating layer. Some evidence of saturation in the ultraviolet end of the spectrum was observed at the highest densities studied but in all other cases the gas appeared to be optically thin.

In the cases studied the radiation is the sum of contributions from overlapping bands and continua, and an unfolding procedure had to be used to isolate the contributions from individual sources. The success of this procedure is based on the fact that the relative contribution to the total radiation from individual bands is a function of wavelength, temperature and density, and it was therefore possible to select conditions under which the radiation from a single band could be isolated by subtracting the contribution due to other sources. The criteria for selection were that at least 50% of the radiation be due to the band under study and that the calculated *f*-numbers be independent of temperature, density, and wavelength over an appropriate range. The procedure is outlined below.

KRAMERS RADIATION FROM O^-

A preliminary step in the analysis was to subtract a small contribution due to the Kramers radiation from O^-. This is composed of parts denoted free-free and free-bound radiation and associated respectively with scattering and capture of electrons by O.

The free-free radiation has been studied in the infrared by Wentink *et al.* (*31*) who found that for an optically thin gas their data could be satisfactorily fitted with an expression of the form:

$$\frac{dI}{dA\,d\Omega\,d\lambda} = Z^2 \cdot \frac{16\pi}{3\sqrt{3}} \cdot \frac{e^6}{mc^2}\,(2\pi mkT)^{-1/2}\lambda^{-2}[\mathrm{O}][e]le^{-hc/kT\lambda} \tag{9}$$

with $Z^2 = 0.04$.

The free-bound radiation may be inferred using detailed balancing arguments from the photodetachment cross section, σ, for O^-. The result for an optically thin gas is:

$$\frac{dI}{dA\,d\Omega\,d\lambda} = \sigma \cdot 2hc^2\lambda^{-5}[\mathrm{O}^-]le^{-hc/kT\lambda}. \tag{10}$$

The cross section, σ, has been measured by Branscomb *et al.* (*27*) from the threshold to about 4000A. A theoretical (*32*) curve which fits this experimental data and predicts the absorption at shorter wavelengths is shown in Fig. 22.

O_2 SCHUMANN–RUNGE BANDS

The *f*-number for the Schumann–Runge bands of O_2 was deduced from the data on pure oxygen shown in Fig. 14. The contribution from Kramers radiation

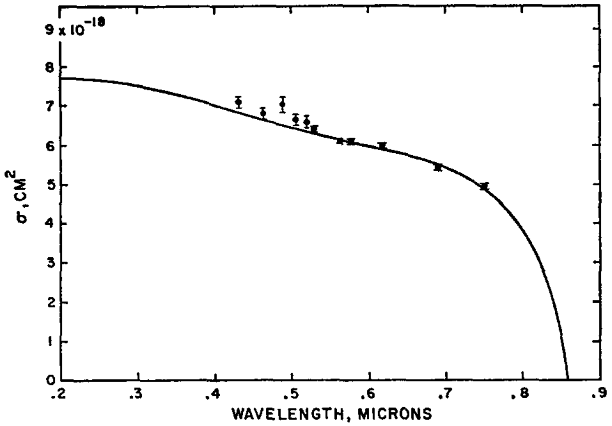

FIG. 22. Photodetachment cross section for O^-. The experimental points are those measured by Branscomb and co-workers. The curve was computed by Kivel and is based on work by Klein and Brueckner.

was subtracted out using Eqs. (9) and (10) and the f-number was then computed from the residue using Eq. (8). The value obtained for the wavelength range 3300 to 4700A was $f = 0.028$ with an rms dispersion of ± 0.008. Within the range of values covered there was no significant variation with wavelength, temperature or density.

NO β BANDS

The f-number for the NO β bands was deduced from selected portions of the data on air shown in Figs. 15, 16b, 16c, 17b, and 17c after subtraction of the contribution from O^- Kramers radiation and the O_2 Schumann–Runge bands. The value obtained for the wavelength interval 3500 to 5000A was $f = 0.006 \pm 0.002$ with no significant dependence on wavelength, temperature, or density.

NO γ BANDS

The f-number for the NO γ bands was determined from the data on air shown in Figs. 16a and 17a after subtraction of the contribution from the sources previously discussed. The value obtained for the wavelength interval 2500 to 2700A was $f = 0.001 \pm 0.0005$ with no significant dependence on wavelength, temperature, or density.

N_2 SECOND POSITIVE BANDS

The f-number for the N_2 second positive bands was determined from the data on air shown in Figs. 16a, 17a, and 18 after subtraction of the contribution from the sources previously discussed. The value obtained for the wavelength interval 2900 to 3300A was $f = 0.09 \pm 0.03$ with no significant dependence on wavelength, temperature, or density.

N_2^+ FIRST NEGATIVE BANDS

The *f*-number for the N_2^+ first negative bands was determined from the data on air shown in Figs. 16c, 17c, and 18 after subtraction of the contribution from the sources previously discussed. The value obtained for the wavelength interval 3300 to 4500A was $f = 0.18 \pm 0.07$ with no significant dependence on wavelength, temperature, and density.

N_2 FIRST POSITIVE BANDS

The *f*-number for the N_2 first positive bands was computed from the data of Figs. 16d, 17d, and 18 after subtraction of the contribution from the sources previously discussed. This band is the principal source in the wavelength interval 6000 to 10,000A and a significant variation in the *f*-number was observed. This is in agreement with the work of Nicholls *et al.* (*9*) who studied the variation with internuclear spacing of the matrix element $| R |$ appearing in the definition of the *f*-number. Their results imply that the *f*-number for the N_2 first positive bands can be represented in the form.

$$f = f_{00} \frac{\lambda_{00}}{\lambda} e^{-6(\langle r \rangle - \langle r_{00} \rangle)} , \tag{11}$$

where f_{00} is a true constant, λ_{00} is the wavelength of the 0, 0 transition, and $\langle r_{00} \rangle$ is the mean of the equilibrium internuclear spacings for the upper and lower potential curves.

The correlation between $\langle r \rangle$ and λ is remarkably close and is shown in Fig. 23. For $\langle r_{00} \rangle = 1.25$A and $\lambda_{00} = 10460$A, Eq. (11) gives a satisfactory representation of the observations with $f_{00} = 0.025 \pm 0.008$.

RECONSTRUCTION OF RADIATION

The comparison of theory and experiment is shown by the curves in Figs. 14 to 18. In general the agreement is within the scatter of the experimental points. There are, however, a number of minor discrepancies which require explanation. The first of these, seen in Figs. 17a and 17b, is the tendency of the theory to overestimate the radiation at high emissivities. This is attributed to self-absorption of the radiation in the gas sample. If the value of line width to spacing is known a correction for this effect may be made. Alternatively the value of the width to spacing ratio may be estimated from the value of the emissivity at which the radiation departs from the theory. Unfortunately neither our knowledge of the width to spacing ratio nor the quality of the experimental data seemed to justify a more thorough analysis of this effect. The second discrepancy, seen in Figs. 16d and 17d, is the tendency of the theory to underestimate the radiation at 6500A. The issue here is confused because two atomic lines, one from H (present as an impurity) and the second from N, were inadvertently included in the wavelength interval studied. The final discrepancy is that seen in Fig. 18 in the wave-

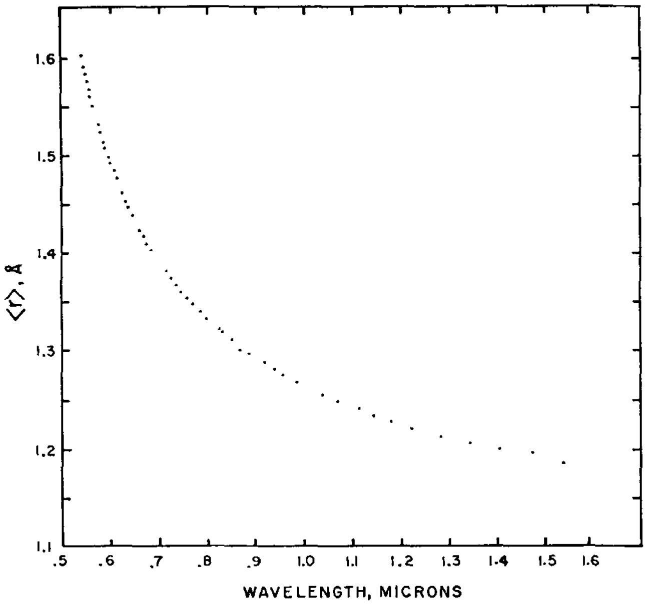

FIG. 23. Correlation of internuclear separation and wavelength of radiation as given by Turner and Nicholls for the N_2 first positive bands. See text for explanation of use.

length region around 5500A where the theory again underestimates the radiation. This is a region in which radiation from the tails of N_2^+ first negative, N_2 second positive and NO β bands are important and a possible explanation may be that the functions, $\langle\varphi\rangle_{\Delta\lambda}$, describing the distribution of radiation are inaccurate on their tails due to the incomplete tables of Condon factors used.

In concluding this discussion we note that any or all of the discrepancies mentioned above may be an indication that sources other than those considered are contributing to the radiation. However, the fact that plausible explanations can be found in other considerations rules out the possibility of a definitive statement on this point. One source of particular interest which one might expect to be important at low temperatures and high densities is NO_2 and it is conceivable that some of the observed discrepancies may be associated with radiation from this molecule. A second source important at high temperatures and low densities is Kramers radiation from atomic and molecular ions. Estimates of the radiation from this source have been made assuming an effective Z of one and it appears to be negligible for the conditions of the present experiment.

COLLISION LIMITING OF RADIATION

In the interpretation of our results the assumption of local thermodynamic equilibrium has been made. Evidence that the major adjustment in energy among the internal degrees of freedom of the gas has occurred is fairly easy to obtain. The fact that the radiation is constant for incident shocks and rises linearly for reflected shocks shows that the temperature of the gas is not changing appreciably. Another indication is that the ratio of the reflected and incident shock speeds is correctly given by the equilibrium theory. The fact that the major adjustment in energy has occurred, however, does not guarantee that the highly excited states from which the radiation originates are in equilibrium. An optically thin gas sample is out of equilibrium due to unbalanced energy loss by radiation and these states may be more rapidly depopulated by radiation than they can be populated by collisions. If this is the case the radiation is said to be "collision limited." Under collision limited conditions one may have steady state radiation at a value considerably less than the equilibrium value.

One method of distinguishing between equilibrium and collision limited radiation is to study the absorption coefficient. Under equilibrium conditions, application of detailed balancing arguments requires emission and aborption coefficients to be related by the equation

$$\epsilon_\lambda = (1 - e^{-\mu_\lambda' l}). \tag{12}$$

Failure to satisfy this relation may indicate collision limiting of the radiation. Unfortunately, under conditions where one would expect collision limiting to occur in shock tubes the absorption is so small that it cannot be easily measured.

An alternative procedure, employed in the case of the present experiments, is to study the density dependence of the radiation. If the population of the radiating state is to be maintained by collision processes then the rate of depopulation of this state by radiation must be small compared to the rate of depopulation by collisions. Assuming deactivation to occur in a binary collision with a particle, X, we can write as a necessary condition for equilibrium radiation:

$$\frac{1}{\tau_r}[B] \ll \sigma_{BX} v_{BX} [B][X], \tag{13}$$

where τ_r is the radiative lifetime of the radiating state, $[B]$ is the concentration of particles in the radiating states, σ_{BX} is the cross section for deactivation by collision with X, v_{BX} is the mean velocity for the collisions between B and X, and $[X]$ is the concentration of X. Introducing Γ_X, by means of the equation:

$$[X] = 2.7 \times 10^{19} \frac{\rho}{\rho_0} \Gamma_X, \tag{14}$$

we may write Eq. (13) in the form:

$$\sigma_{BX} \gg \sigma_c \equiv 9 \times 10^{-18} \frac{f}{\lambda^2} \frac{\rho_0}{\rho} \left(\frac{10^4}{T}\right)^{1/2} M_{BX}{}^{1/2} \frac{1}{\Gamma_X}, \tag{15}$$

where λ is the wavelength in microns, T is the temperature in °K, and M_{BX} is the reduced atomic mass for collision of B and X. The cross section σ_c is plotted

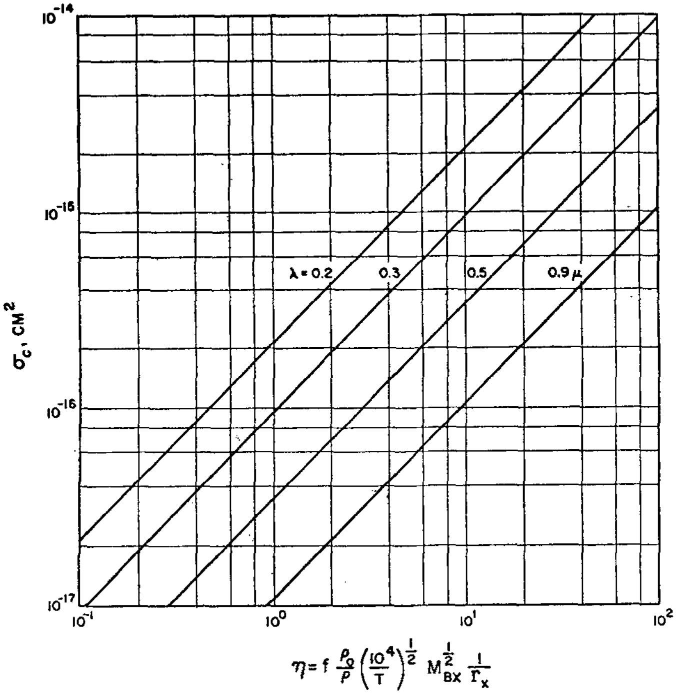

FIG. 24. Collisional deactivation cross section required to maintain radiation at the equilibrium level as a function of the parameter η for several values of wavelength.

as a function of the parameter

$$\eta = f \frac{\rho_0}{\rho}\left(\frac{10^4}{T}\right)^{1/2} M_{BX}^{1/2} \frac{1}{\Gamma_X}$$

for several values of λ in Fig. 24. If the deactivation cross section, σ_{BX} , is known, Eq. (15) defines the density range over which the equilibrium assumption *may* be valid. If the deactivation cross section is not known, Eq. (15) implies that it may be measured by determining the density at which the radiation begins to fall below the equilibrium value.

At the present time, cross sections for deactivation of the radiating species important in air are unknown. The experimental indication (*33*) is that diatomic molecules deactivate electronic states with cross sections of the order of 5×10^{-15} cm^2 (and on occasion they are even larger). The electronic energy goes into exciting the vibration of the diatomic molecule. In view of this data we may estimate the critical densities above which equilibrium radiation may be expected for the temperature range of interest by setting $\sigma_{BX} = 10^{-15}$ cm^2 and giving Γ_X its maximum value of 2. These are shown in Table III. It will be noted that in some cases these critical densities are less than a factor of 10 greater than those

TABLE III

DENSITIES BELOW WHICH RADIATION FROM VARIOUS BAND SYSTEMS IS "COLLISION LIMITED" BASED ON A DE-EXCITATION CROSS SECTION OF 10^{-15} cm^2

Band system	Critical density $\div \rho_0$
O_2 Schumann–Runge	0.0055
NO γ	0.0009
NO β	0.0013
N_2 first positive	0.0010
N_2 second positive	0.031
N_2^+ first negative	0.018

for which measurements were made in the present experiments. Since a satisfactory fit to the data, down to the lowest densities, was obtained by assuming equilibrium populations, we can conclude that, averaged with respect to all particles, the cross sections for deactivation by collision are of the order of 10^{-15} cm^2.

A preliminary attempt was made to reach a collision limited situation in pure oxygen. The results are shown in Fig. 25 where the apparent electronic f-number is plotted as a function of density for a temperature in the neighborhood of 4000°K. For densities from $\rho = 0.02$ to $0.2\ \rho_0$ the f-numbers are constant within the scatter of the data. At higher densities there is a fall-off which can be attributed to the fact that self-absorption is becoming important. There is no indication of a fall off at low density, however. It was not possible to extend the data

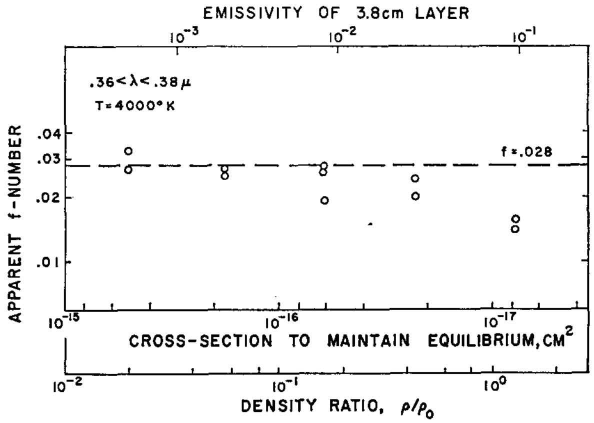

FIG. 25. Apparent f-number for the O_2 Schumann–Runge bands as a function of density. The dashed line shows our best estimate of the true value of f from all measurements. The fall-off in the apparent f-number at high densities can be attributed to self-absorption. There is no evidence of a fall-off at low densities, indicating a collisional deactivation cross-section of at least 10^{-15} cm^2.

to lower densities due to the fact that the test time became too short to allow the radiation to relax to a steady state value. The results as they stand imply a lower limit on the deexitation cross section for the O_2 Schumann–Runge bands of 10^{-15} cm^2. The study of the collision limiting of radiation is a very promising tool for the determination of deactivation cross sections and further work on this problem is contemplated.

DISCUSSION

There are a number of previously published reports with which we may compare the present work.

In a letter to the *Journal of Chemical Physics*, Keck *et al.* (*34*) quoted an "effective f-number" of 0.015 for the Schumann–Runge bands of O_2 which is significantly smaller than the value $f = 0.028$ given in the present report. The difference, however, is in the definition of the "effective f-number" of the simplified theory of KMB used in the earlier analysis. The quantity in the present theory which is equivalent to the "effective f-number" is $f\langle\varphi\rangle_{\Delta\lambda}$ which is 0.015 in agreement with the earlier work.

In absorption experiments at 1470A Watanabe and co-workers (*7*) have measured an f-number of 0.16 for the Schumann–Runge bands. Correcting this value for the wavelength-dependent factor contained in the definition of the f-number implies a value of 0.06 at a wavelength of 4000A to be compared with our value of 0.028. The remainder of the difference could be due to a fall off in f-number with increasing nuclear separation similar to that observed for the N_2 first positive bands (*9*) but might also be attributed to experimental error.

The radiative properties of shock-heated air have also been studied by Wurster *et al.* (*17*). They give a detailed curve of the absorption coefficient of air at a temperature of 4380°K and density of 4.0 ρ_0 over the wavelength range 2590 to 2880A which implies an average value of 0.8 cm^{-1} for the interval 2600 to 2800A. The present work indicates that under their conditions the contributions to the absorption coefficient from the O_2 Schumann–Runge, NO β and NO γ bands are respectively 0.38, 0.20, and .04 cm^{-1} giving a total of 0.62 cm^{-1}. Considering the difficulties inherent in shock tube experiments of this type the agreement is considered excellent.

The NO γ band absorption coefficient has recently been measured by Weber and Penner (*6*) using self-broadening to eliminate rotational structure. They obtained a value for the electronic f-number of 0.0025. More recently Dieke and co-workers (*35*) at Johns Hopkins University using high resolution spectroscopy have indicated in a progress report that the value might be somewhat smaller (0.0013). The latter value is favored by our results.

To conclude, we believe that the present work provides a fairly complete picture of the radiative properties of oxygen, nitrogen, and air in the temperature range 4000 to 9000°K. In general the comparison with other work is very satisfactory and indicates that the techniques employed are sound. It is clear that the shock tube has a tremendous potential for spectroscopic problems and, in particular, for the determination of *f*-numbers. The exploitation of this potential is sure to add much to our understanding of these problems.

ACKNOWLEDGMENT

The authors wish to acknowledge the enthusiastic support given this work by A. R. Kantrowitz, Director of the Avco Research Laboratory, and the many members of the staff who contributed to the work. We are especially indebted to D. Teare who carried out many of the shock tube calculations, R. Prescott who designed the optical equipment, J. Trask who was responsible for running the shock tube, P. Gorenstein, R. Carbone and W. Planet who assisted with general experimental details, and K. Bailey who programmed the reduction of the data. We should also like to thank Avco consultants and friends R. Meyerott, H. Bethe, G. Dieke, H. Mayer and S. S. Penner for many helpful discussions and suggestions.

APPENDIX A. APPROXIMATION TO THE CONDON FACTORS FOR O_2 SCHUMANN-RUNGE SYSTEM

Condon factors for the O_2 Schumann–Runge bands have not been calculated for large values of v'. For this reason a simple approximation was used to estimate these probability factors based on the empirical observation that in the case of a similar band system, the NO β bands, the Condon factors for a given upper state plotted as a function of the classical turning point for the lower state looked very much like the wave function for the upper state. In this approximation the Condon factors $q_{v'v''}$ are given simply as:

$$q_{v'v''} = \frac{\gamma_{v''} \,|\, \psi_{v'}(r_{v''}) \,|^2}{\sum_{v''} \gamma_{v''} \,|\, \psi_{v'}(r_{v''}) \,|^2},$$

where

$$\gamma_{v''} = \left[\left(\frac{\partial V}{\partial r} \right)_{r=r_{v''}} \right]^{-1}$$

is a factor proportional to the time a molecule in the v'' state spends in the vicinity of the classical turning point, $r_{v''}$, and $\psi_{v'}$ $(r_{v''})$ is the Morse wave function for the v' state evaluated at $r_{v''}$. The approximation is equivalent to replacing the wave function in the lower state by a delta function at the classical turning point and normalizing so that the sum rule

$$\sum_{v''} q_{v'v''} = 1$$

is obeyed. The approximation was checked in the case of the NO β bands by comparing it with results of KMB. Except for a small shift in the positions of the maxima and minima of the curve of $q_{v'v''}$ versus v'' the agreement was remarkably good and indicates that no significant errors should be involved in the use of the approximation for calculating the average emission of similar bands, particularly at high temperatures where large values of v' are involved.

RECEIVED: January 13, 1959

REFERENCES

1. H. E. WHITE, "Introduction to Atomic Spectra." McGraw Hill, New York, 1934.

2. G. HERZBERG, "Spectra of Diatomic Molecules," 2nd ed. Van Nostrand, New York, 1950.

3. H. BETHE, Handbuch der Physik, 2nd ed., Vol. 24. Springer, Berlin, 1933.

4. B. KIVEL, H. MAYER, AND H. BETHE, *Annals of Physics* **2,** 57 (1957).

5. R. E. MEYEROTT, LMSD-2264, Lockheed, Palo Alto, Calif., 1957.

6. D. WEBER AND S. S. PENNER, *J. Chem. Phys.* **26,** 860 (1957).

7. K. WATANABE, M. ZELIKOFF, AND E. C. Y. INN, Absorption Coefficients of Several Atmospheric Gases, G. R. D.-A. R. D. C., Cambridge, 1953.

8. R. W. DITCHBURN, *Proc. Roy. Soc.* **236,** 216 (1956).

9. R. G. TURNER AND R. W. NICHOLLS, *Can. J. Phys.* **32,** 468 (1954).

10. E. RESLER, S. C. LIN, AND A. KANTROWITZ, *J. Appl. Phys.* **23,** 1390 (1952).

11. R. N. HOLLYER, JR., A. C. HUNTING, O. LAPORTE, AND E. B. TURNER, *Nature* **171,** 395 (1953).

12. H. E. PETSCHEK, P. H. ROSE, H. S. GLICK, A. KANE, AND A. KANTROWITZ, *J. Appl. Phys.* **26,** 83 (1955).

13. E. B. TURNER, AFOSR-TN-56-150, ASTIA Document No. AD 86309, Engineering Research Institute, The University of Michigan, Ann. Arbor, 1956.

14. A. C. KOLB, AFOSR-TN-57-8, ASTIA Document No. AS 115 040, Engineering Research Institute, The University of Michigan, Ann Arbor, 1957.

15. G. E. SEAY, LAMS-2125, Los Alamos Scientific Lab., Los Alamos, New Mexico, 1957. G. E. SEAY AND L. B. SEELY, *Bull. Am. Phys. Soc.* Ser. II, **2,** 227 (1956).

16. I. SH. MODEL', *J. Exptl. Theoret. Phys. (U.S.S.R.)* **32,** 714 (1957), *Soviet Phys. JETP* **5,** 589 (1957).

17. W. H. WURSTER, H. S. GLICK, AND C. E. TREANOR, QM-997-A-1, Cornell Aeronautical Laboratory, Buffalo, New York, 1957.

18. W. H. WURSTER AND H. S. GLICK, *J. Chem. Phys.* **27,** 1218 (1957).

19. J. G. CLOUSTON AND A. G. GAYDON, *Nature* **180,** 1342 (1957); A. R. FAIRBAIRN AND A. G. GAYDON, *Proc. Roy. Soc.* **A239,** 464 (1957).

20. R. W. NICHOLLS AND W. H. PARKINSON, *J. Chem. Phys.* **26,** 423 (1957).

21. H. MARK, AFOSR-TN-57-345, Cornell University, Ithaca, N. Y., 1957.

22. P. H. ROSE AND W. NELSON, RR-24, Avco Research Laboratory, Everett, Mass., 1958.

23. S. FELDMAN, Hypersonic Gas Dynamic Charts for Equilibrium Air, (Avco Research Laboratory, Everett, Mass., 1957.

24. F. R. GILMORE, RM-1543, The Rand Corporation, Santa Monica, California, 1955.

25. J. G. LOGAN, JR., AD-1052-A-1, Cornell Aeronautical Laboratory, Buffalo, N. Y., 1956.

26. J. CAMM, to be submitted to Rev. Sci. Instr.

27. L. M. BRANSCOMB, B. S. BURCH, S. J. SMITH, AND S. GELTMAN, Phys. Rev. **111,** 504 (1958).

28. J. C. DEVOS, *Physica* **20,** 690 (1954).

29. J. EULER, *Sitzber. heidelberg Akad. Wiss. Math.-Naturw. Kl.* **No. 4,** 413 (1956–57).

30. W. R. JARMAIN AND W. R. NICHOLLS, *Can J. Phys.* **32,** 201 (1954); W. R. JARMAIN, P. A.

Fraser, and R. W. Nicholls, *Astrophys. J.* **118,** 228 (1953); **119,** 286 (1954); **122,** 55 (1955).

31. T. Wentink, Jr., W. Planet, P. Hammerling, and B. Kivel, *J. Appl. Phys.* **29,** 742 (1958).

32. M. M. Klein and K. A. Brueckner, *Phys. Rev.* **111,** 1115 (1958); S. C. Lin and B. Kivel, *Phys. Rev.* (to be published).

33. H. S. W. Massey and E. H. S. Burhop, Electronic and Ionic Impact Phenomena," Oxford Univ. Press, London and New York, 1952.

34. J. Keck, J. Camm, and B. Kivel, *J. Chem. Phys.* **28,** 723 (1958).

35. G. H. Dieke, private communication.